Path Following Control with Slip Compensation on Loose Soil for Exploration Rover

Genya Ishigami, Keiji Nagatani, and Kazuya Yoshida
Department of Aerospace Engineering
Tohoku University
Aoba 6-6-01, Sendai, 980-8579, Japan
{ishigami, keiji, yoshida}@astro.mech.tohoku.ac.jp

***Abstract*— In this paper, a path following control strategy for lunar/planetary exploration rovers is described, taking into account slip motion of the rover. It is determined that the slip motion of each wheel of the rover must be increased and cannot be neglected when the rover travels on loose soil. Because of slip, following an arbitrary path on loose soil is a difficult task. In order to improve this situation, the authors have developed a path following algorithm with slip compensation. In this algorithm, both steering and driving maneuvers of the rover are derived not only to follow an arbitrary path, but also simultaneously compensate for the slip. The performance of the path following strategy is confirmed through numerical simulation using the wheel-and-vehicle model elaborated in our previous research. The slip motion of the wheel is also addressed, based on a terramechanics approach. The proposed path following algorithm shows better performance than traditional control without slip compensation in the simulation.**

I. INTRODUCTION

During the last decade, progress in space exploration technology has significantly advanced us to perform various scientific missions, such as investigations about the origin of the solar system. Particularly, the effectiveness of a surface exploration robot (*Rover*) in such missions has been recently demonstrated by both of NASA's Sprit and Opportunity rovers since 2004 [1]. Because of growing demand for more complex missions, rovers are expected to travel much longer distances, climb hills and traverse slopes. A considerable amount of research has been published on various subjects dealing with exploration rovers [1]-[4].

The surface of a planetary body, such as the Moon or Mars, is covered with loose soil, boulders, rocks or stones spread over the terrain. On such challenging terrain, the rover must design a motion planning to avoid obstacles autonomously or semi-autonomously. Slipping of the rover wheels in loose soil makes following a given path a difficult task. In order to deal with path following problems on loose soil, it is important to model the slip behavior.

There are a great number of papers and books regarding path following issues [5]-[8]. For example, Rezaei et al. investigated an on-line path following strategy combined with a SLAM algorithm for a car-like robot in outdoor environments [7]. Helmick et al. developed a path following algorithm with slip compensation using visual odometry and a Kalman filter [8]. Most of this research, however, does not consider wheel slip. For this reason, it is not possible to employ conventional approaches to the issue of path following on loose soil.

The mechanics of a slipping wheel on loose soil has been studied in the field of *Terramechanics* [9]-[14]. In this field, analysis of wheel-soil interaction mechanisms and modeling of stress distributions underneath a wheel on loose soil have been well investigated [9][10]. Iagnemma et al. applied these terramechanics models to the issues of planetary rovers [11]. The authors have also previously elaborated the wheel-and-vehicle model to deal with traveling characteristics of rovers [12]-[14].

In this paper, applying our background in terms of dynamic slip motion, a path following control strategy with slip compensation on loose soil is addressed. As previously described, the slip motion of a rover become relatively large on loose soil. There are three main slip motions: a vehicle's sideslip and both longitudinal and lateral slip of a wheel. In conventional path following approaches, these slip motions are assumed to be negligible. Because of this, a kinematic and dynamic model of a vehicle based on such a model also includes minimal slip behavior. A key issue in this research is the development of a control strategy compensating these three types of slip so that a rover can follow an arbitrary path, even on loose soil. In this paper, nonholonomic constraints of a vehicle including the vehicle's sideslip and wheel's lateral slip are addressed. The longitudinal slip is also compensated by controlling the angular velocity of each wheel. The proposed algorithm therefore calculates both steering and driving maneuvers that enable a rover to compensate for slip and also to follow a given path.

The performance of the path following control is confirmed using a dynamic simulation. In the simulation, the dynamic behavior of a rover is modeled with a wheel-and-vehicle model [13]. The slip of wheels is properly addressed, based on the terramechanics approach. The wheel-and-vehicle model has been successfully validated in previous works [13][14]. According to the results of the simulation, the proposed algorithm shows better performance than traditional control which does not consider the effect of slip. In particular, the validity of the proposed control strategy is proved in a slope-traversing situation.

The paper is organized as follows: Section II describes a nonholonomic kinematic model of a vehicle, with taking

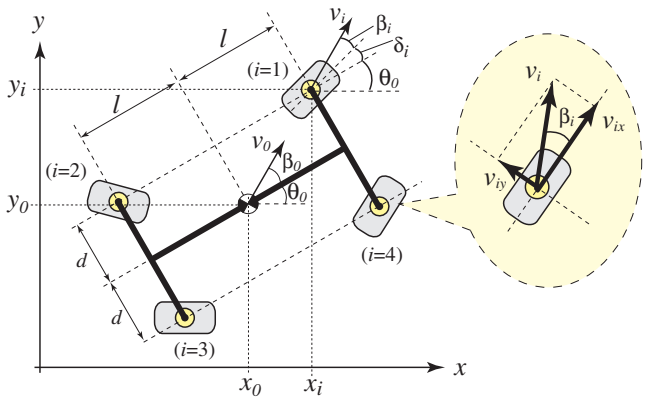

Fig. 1. Kinematic model of 4 wheeled vehicle

into account wheel slip. In Section III, the proposed path following algorithm is introduced, along with the derivation of both desired steering and driving maneuvers respectively. The wheel-and-vehicle model, which includes the dynamic model of a vehicle and the wheel-soil contact model, is presented in Section IV. In Section V, the simulation study and performance of the path following control are described.

II. Nonholonomic Kinematic Model of Vehicle

The nonholonomic kinematic model of a vehicle is addressed in this section. The sideslip of the vehicle and lateral slip of the wheels are taken into account while discussing nonholonomic constraints. To discuss the nonholonomic kinematic model of the vehicle, the following assumptions are considered:

1) the distance between wheels (generally called wheelbase and tread) are strictly fixed.
2) the steering axle of each wheel is perpendicular to the terrain.
3) the vehicle does not consist of any flexible parts. /the vehicle is rigid.

A. Kinematic model with slip angle

A kinematic model of a 4 wheeled vehicle including the slips is shown in Fig. 1. In this model, each wheel has a steering angle δ_i and slip angle β_i. The slip angle, which measures a wheel lateral slip, is calculated by longitudinal and lateral linear velocities v_{ix}, v_{iy} of the wheel as follows:

$$\beta_i = \tan^{-1}(v_{iy}/v_{ix}) \tag{1}$$

The subscript i denotes the wheel ID as shown in Fig. 1. The position and orientation of the center of gravity of the vehicle is defined as (x_0, y_0, θ_0), while (x_i, y_i) gives the position of each wheel. v_0 and v_i are the linear velocities of the vehicle and each wheel, respectively. β_0 denotes the sideslip of the vehicle, which is determined by the same method as (1). l is the longitudinal distance from the center of gravity of the vehicle to the front or rear wheel and d defines the lateral distance from the center of gravity of the vehicle to the left or right wheel. Here, based on previously defined assumptions, l and d are constant values.

B. Nonholonomic constraints

The conventional nonholonomic constraints have been discussed with approximate models such as *Bicycle model* [5]. In this model, a 4-wheeled car-like vehicle is approximated as a 2-wheeled bicycle-like vehicle. A disadvantage of this model is that it is not able to properly deal with slip of the wheels.

The nonholonomic constraints in this research is therefore expressed by the following equation, taking into account wheel slip:

$$\dot{x}_0 \sin\phi_0 - \dot{y}_0 \cos\phi_0 = 0 \tag{2}$$

$$\dot{x}_i \sin\phi_i - \dot{y}_i \cos\phi_i = 0 \tag{3}$$

where, $\phi_0 = \theta_0 + \beta_0$, and $\phi_i = \theta_0 + \delta_i + \beta_i$. Also, geometric constraints between every wheel and the center of gravity of the vehicle are written as:

$$\left.\begin{aligned} x_1 &= x_0 + l\cos\theta_0 - d\sin\theta_0 \\ x_2 &= x_0 - l\cos\theta_0 - d\sin\theta_0 \\ x_3 &= x_0 - l\cos\theta_0 + d\sin\theta_0 \\ x_4 &= x_0 + l\cos\theta_0 + d\sin\theta_0 \end{aligned}\right\} \quad \rightarrow \quad x_i = x_0 + X_i \tag{4}$$

$$\left.\begin{aligned} y_1 &= y_0 + l\sin\theta_0 + d\cos\theta_0 \\ y_2 &= y_0 - l\sin\theta_0 + d\cos\theta_0 \\ y_3 &= y_0 - l\sin\theta_0 - d\cos\theta_0 \\ y_4 &= y_0 + l\sin\theta_0 - d\cos\theta_0 \end{aligned}\right\} \quad \rightarrow \quad y_i = y_0 + Y_i \tag{5}$$

Substituting (4) and (5) into (3), the following matrix form equation is obtained:

$$\boldsymbol{A}_0 \cdot \dot{\boldsymbol{q}}_0 = 0 \tag{6}$$

where,

$$\boldsymbol{A}_0 = \begin{bmatrix} \sin\phi_1 & -\cos\phi_1 & -l\cos(\phi_1-\theta_0) - d\sin(\phi_1-\theta_0) \\ \sin\phi_2 & -\cos\phi_2 & l\cos(\phi_2-\theta_0) + d\sin(\phi_2+\theta_0) \\ \sin\phi_3 & -\cos\phi_3 & l\cos(\phi_3-\theta_0) - d\sin(\phi_3+\theta_0) \\ \sin\phi_4 & -\cos\phi_4 & -l\cos(\phi_4-\theta_0) + d\sin(\phi_4-\theta_0) \end{bmatrix}$$

$$\dot{\boldsymbol{q}}_0 = [\ \dot{x}_0 \quad \dot{y}_0 \quad \dot{\theta}_0\ ]^T$$

Here, it is complicated to derive a null-space vector of the constraints matrix $\boldsymbol{A}_0$ if obtaining the vector $\dot{\boldsymbol{q}}_0$ which satisfies (6). Therefore, a simplified constraints matrix $\boldsymbol{A}_i$ for each wheel is represented instead of $\boldsymbol{A}_0$:

$$\boldsymbol{A}_i \cdot \dot{\boldsymbol{q}}_i = 0 \tag{7}$$

For example, in terms of the front-left wheel ($i = 1$):

$$\boldsymbol{A}_1 = \begin{bmatrix} \sin\phi_1 & -\cos\phi_1 & -l\cos(\phi_1-\theta_0) - d\sin(\phi_1-\theta_0) \\ \sin\phi_0 & -\cos\phi_0 & 0 \end{bmatrix} \tag{8}$$

Using a null-space vector of $\boldsymbol{A}_1$, it is possible to obtain the vector $\dot{\boldsymbol{q}}_1$ satisfying (7):

$$\dot{\boldsymbol{q}}_1 = \begin{bmatrix} \cos\phi_0 \\ \sin\phi_0 \\ \frac{\sin(\delta_1+\beta_1-\beta_0)}{-l\cos(\delta_1+\beta_1) - d\sin(\delta_1+\beta_1)} \end{bmatrix} \cdot v \tag{9}$$

where v can be qualified as the linear velocity of the vehicle, namely v_0. Note that the other constraints matrices $\boldsymbol{A}_2$-$\boldsymbol{A}_4$ are defined as the same fashion as (8). Also the null-space vectors $\boldsymbol{q}_2$-$\boldsymbol{q}_4$ can be formed by the above scheme.

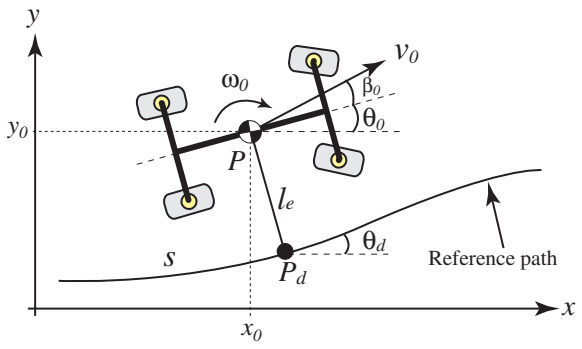

Fig. 2. Illustration of path following control

Additionally, an algorithmic singularity for a steering angle is calculated from (9). The singular steering angle δ_i^* is derived by paying attention to the denominator of the third component in (9):

$$\delta_i^* = \pm \tan^{-1}(l/d) - \beta_i \tag{10}$$

From (10), it is reasonable that the singular steering angle is mainly dominated by a vehicle's configuration, namely l and d. The singular steering angle gives an unstable state, and then the controllability of a vehicle will become worse.

III. Path Following Algorithm with Slip Compensation

In this section, a traditional approach to follow an arbitrary path is recalled, and then a simple strategy to reduce a vehiclefs sideslip of is developed. Also, we propose how to distribute control inputs to both steering and driving axles with taking into account slip compensations.

A. Path following control

The discussion described in the subsection is based on the approach developed in [6]. A general illustration of the path following problem is shown in Fig. 2. The current vehicle's position is denoted by P, the shortest distance projection of P to a reference path is denoted by P_d. Each symbol used in the path following problem is defined as follows:

- s : signed curvilinear distance along the path from an initial point to the point P_d.
- l_e : signed distance between P and P_d (distance error.)
- θ_d : angle between the x-axis and the tangent to the path at P_d.
- c : curvature of the path at P_d (vehicle's desired orientation.)
- θ_e : orientation error (= $\theta_0 - \theta_d$.)

Using the variables s, l_e and θ_e, the kinematic state equations can be formulated as:

$$\left.\begin{aligned} \dot{s} &= v_0 \cos(\theta_e + \beta_0)/(1 - c \cdot l_e) \\ \dot{l_e} &= v_0 \sin(\theta_e + \beta_0) \\ \dot{\theta_e} &= \omega_0 - c \cdot v_0 \cos(\theta_e + \beta_0)/(1 - c \cdot l_e) \end{aligned}\right\} \tag{11}$$

In the path following problem, a feedback control law is employed to satisfy both $l_e \to 0$ and $\theta_e \to 0$. Then, the control objectives are realized by the use of one control variable, which is a turning angular velocity of vehicle $\omega_0 (= \dot{\theta}_0)$ [6]. Thus, considering a linear state feedback control when v_0 is constant and not be zero, a path following control input u_p is given by:

$$u_p = -k_1 v l_e - k_2 |v| \theta_e - k_3 |v| \dot{\theta_e} \tag{12}$$

where, k_1, k_2 and k_3 are control gains.

B. Sideslip control

On loose soil, a vehicle has a certain amount of sideslip, which is denoted by β_0. It is simply deduced that the sideslip phenomenon must lead to an unexpected orientation error in the path following issue. Therefore, we consider that the sideslip can be reduced by another control objective, namely $\beta_0 \to 0$. Combining with the control input u_p represented in (12), another control input u_β, which decreases the sideslip, is modeled as:

$$u_\beta = k_4 \beta_0 + k_5 \omega_0 \tag{13}$$

where, k_4 and k_5 are control gains.

Note that these two control inputs, u_p and u_β, are selectively distributed to both steering and driving axles: for example, front wheel pair is controlled to follow a path by u_p, while rear pair compensates a sideslip by u_β.

C. Steering and driving maneuvers with slip compensation

The control inputs have to be distributed into several actuators that are mainly located on steering and driving units.

1) Steering maneuvers: A desired steering angle of each wheel δ_{di} is elaborated as follows. First, by transforming the nonholonomic constraints, (3), we can obtain as:

$$\delta_{di} = \tan^{-1}(\dot{y}_i / \dot{x}_i) - \theta_d - \beta_i \tag{14}$$

Substituting (4) and (5) into (14), δ_{di} is derived by the following equation:

$$\delta_{di} = \tan^{-1}\left[\frac{\dot{y}_{d0} - \dot{Y}_i(\dot{\theta}_d)}{\dot{x}_{d0} - \dot{X}_i(\dot{\theta}_d)}\right] - \theta_d - \beta_i \tag{15}$$

where, $\dot{x}_{d0}$ and $\dot{y}_{d0}$ are desired linear velocities to each direction. Also, $\dot{X}_i$ and $\dot{Y}_i$ become a function of $\dot{\theta}_d$, which is desired turning angular velocity of vehicle. Then, desired control inputs to (15) are eventually summarized as follows:

$$[\ \dot{x}_{d0}\ \ \dot{y}_{d0}\ \ \dot{\theta}_d\ ]^T = [\ v_{d0}\cos\theta_d\ \ v_{d0}\sin\theta_d\ \ u_p(\text{or } u_\beta)\ ]^T \tag{16}$$

where, v_{d0} is a desired linear velocity of the center of gravity of a vehicle. Note that, the desired velocity v_{d0} and control gains, such as k_1-k_5, have to be chosen as avoiding the singular steering angle as mentioned in (10).

2) Driving maneuvers: The driving maneuver is defined as a control of wheel angular velocity ω_i. The relationship between ω_i and a wheel linear velocity v_i is written as:

$$\omega_i = v_i \cos\beta_i / r \tag{17}$$

where, r is a wheel radius. Also, v_i is expressed by $\dot{x}_i$:

$$v_i = \dot{x}_i / \cos\phi_i \tag{18}$$

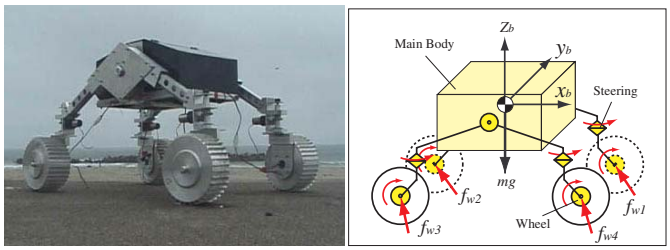

(Rover test bed) (Vehicle dynamics model)

Fig. 3. Rover test bed and vehicle dynamics model

Based on (4), a desired wheel angular velocity ω_{di} is finally derived using $\dot{x}_i = \dot{x}_0 + \dot{X}_i$:

$$\omega_{di} = \frac{\dot{x}_{d0} + \dot{X}_i(\dot{\theta}_d)}{r\cos\phi_i} \cdot \cos\beta_i \tag{19}$$

Additionally, the desired wheel angular velocity has to be adjusted to compensate the longitudinal slip of wheel. The slip in the longitudinal direction is defined as *slip ratio* s_i, which is calculated as a function of the longitudinal linear velocity v_{ix} and the circumference velocity of a wheel $r\omega_i$:

$$s_i = \begin{cases} (r\omega_i - v_{ix})/r\omega_i & (r\omega_i > v_{ix} : \text{driving}) \\ (r\omega_i - v_{ix})/v_{ix} & (r\omega_i < v_{ix} : \text{braking}) \end{cases} \tag{20}$$

The slip ratio takes a value between -1 and 1. Thus, an improved desired angular velocity $\hat{\omega}_{di}$ compensating the longitudinal slip is rewritten as follows:

$$\hat{\omega}_{di} = \omega_{di}/(1 - (s_{ref} - s_i)) \tag{21}$$

where, s_{ref} means a reference slip ratio to regulate the longitudinal slip of a wheel. In our approach, the value of s_{ref} is given between 0.1 and 0.3, where a wheel traction is obtained the most efficient value referring to our previous researches.

IV. Wheel-and-Vehicle Model

In order to validate the proposed path following algorithm, the dynamics simulation has been carried out. The wheel-and-vehicle model for the simulation consists of two models: the vehicle dynamics model and the wheel-soil contact model.

In this research, the vehicle in the simulation is referred to our rover test bed which was developed by the authors, as shown in Fig. 3. The 4-wheeled rover test bed weighs about 35 [kg] in total. The rover has 0.48 [m] in the wheelbase and 0.34 [m] in tread. Each wheel of the rover has an active steering DOF.

A. Vehicle dynamics model

The vehicle dynamics model shown in Fig. 3 has to be completely equivalent to the rover test bed. The dynamic motion equation of the vehicle is generally written as:

$$\boldsymbol{H}\begin{bmatrix} \dot{\boldsymbol{v}}_0 \\ \dot{\boldsymbol{\omega}}_0 \\ \ddot{\boldsymbol{q}} \end{bmatrix} + \boldsymbol{C} + \boldsymbol{G} = \begin{bmatrix} \boldsymbol{F}_0 \\ \boldsymbol{N}_0 \\ \boldsymbol{\tau} \end{bmatrix} + \boldsymbol{J}^T \begin{bmatrix} \boldsymbol{F}_e \\ \boldsymbol{N}_e \end{bmatrix} \tag{22}$$

where the symbols used in the above equation are listed as:

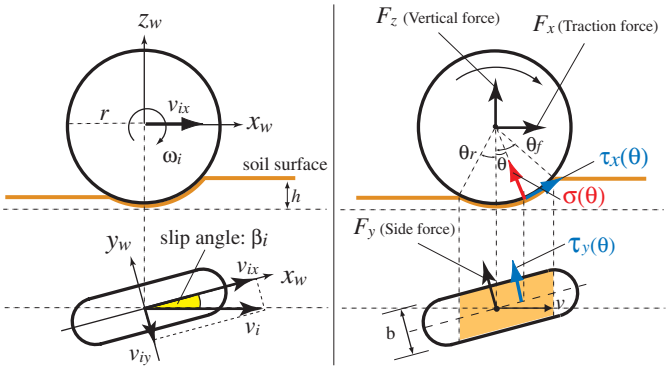

Fig. 4. Wheel-soil contact model

- $\boldsymbol{H}$: inertia matrix of the vehicle.
- $\boldsymbol{C}$: velocity depending term.
- $\boldsymbol{G}$: gravity term.
- $\boldsymbol{v}_0$: linear velocity of the main body.
- $\boldsymbol{\omega}_0$: angular velocity of the main body.
- $\boldsymbol{q}$: angle of each joint of the vehicle.
- $\boldsymbol{F}_0$: forces acting at the main body.
- $\boldsymbol{N}_0$: torques acting at the main body.
- $\boldsymbol{\tau}$: torques acting at each joint of the vehicle.
- $\boldsymbol{J}$: Jacobian matrix.
- $\boldsymbol{F}_e$ $= [\boldsymbol{f}_{w1}, \cdots, \boldsymbol{f}_{wm}]$: external forces acting at each wheel (m is the number of wheels.)
- $\boldsymbol{N}_e$: torques acting at each wheel

Note that, each external force $\boldsymbol{f}_{wi}$ is derived by the wheel-soil contact model, as mentioned in (23)-(25) later.

The (22) is general and can be applied to a vehicle with any configurations. Specific parameters for the rover kinematics and dynamics are identified from the test bed and used in the simulation. The motion of the rover with given traveling and steering conditions is numerically calculated by solving (22) successively. The wheel-and-vehicle dynamics model has been successfully validated in our previous researches [13][14].

B. Wheel-soil contact model

A general force model for a rigid wheel traveling on loose soil is presented in Fig. 4. The wheel coordinate system is defined as a right-hand frame as shown in Fig. 4, where the longitudinal direction is denoted by x_w, the lateral direction by y_w, and the vertical direction by z_w.

Based on the terramechanics approach, wheel contact forces, such as a drawbar pull F_x, a side force F_y and a vertical force F_z, are able to obtain in the same fashion [9][10][12]:

$$F_x = rb\int_{\theta_r}^{\theta_f} \{\tau_x(\theta)\cos\theta - \sigma(\theta)\sin\theta\}d\theta \tag{23}$$

$$F_y = \int_{\theta_r}^{\theta_f} \{rb\cdot\tau_y(\theta) + R_b\cdot(r - h(\theta)\cos\theta\}d\theta \tag{24}$$

$$F_z = rb\int_{\theta_r}^{\theta_f} \{\tau_x(\theta)\sin\theta + \sigma(\theta)\cos\theta\}d\theta \tag{25}$$

where, b is a width of the wheel, and $\sigma(\theta)$ is the normal stress underneath the wheel. $\tau_x(\theta)$ and $\tau_y(\theta)$ mean shear stresses in

the longitudinal and lateral direction of the wheel. Also, the contact region of the wheel on loose soil is determined by the entry angle θ_f and the exit angle θ_r. In addition, R_b is modeled as a reaction resistance generated by the bulldozing phenomenon on a side face of the wheel [12]. R_b is given as a function of a wheel sinkage h.

Note that, σ, τ_x and τ_y are key components to derive the wheel forces, and, they are dominated by slip ratio and slip angle, respectively. The contact region of the wheel is also depended on slip behaviors. Thus, the wheel-soil contact model can deal with the slipping wheel. The contact model has been successfully verified in [12]-[13].

V. Simulation Study

Path following simulations were conducted along with comparisons of the results between the control with and without slip compensations. The performance of the proposed control strategy is discussed based on distance and orientation errors. In this paper, the simulation in a case when the rover traverses an inclined surface (slope) is focused on.

A. Simulation procedure

Using the wheel-and-vehicle model as mentioned in Section IV, the path following simulation is executed as follows:

1) Generate a reference path from the initial to the final posture of the vehicle, and define the initial conditions of the simulation.
2) Derive the path following control inputs u_p and u_β using (12) and (13).
3) Calculate the desired steering angles δ_{di} and angular velocities $\hat{\omega}_{di}$ based on (15) and (21).
4) Calculate the external forces $\boldsymbol{f}_{wi}$ acting to each wheel using the wheel-soil contact model ((23)-(25)).
5) Determine $\boldsymbol{F}_0$, $\boldsymbol{N}_0$, $\boldsymbol{F}_e$, $\boldsymbol{N}_e$ and $\boldsymbol{\tau}$.
6) Slove (22), then obtain the rover position, orientation and velocities.
7) Calculate the sideslip of the rover, slip ratios and slip angles of each wheel, then return to the step 2).

B. Simulation condition

In the simulation, the surface is supposed to be evenly covered with the *Lunar Regolith Simulant*, which is simulated lunar surface soil in terms of similar material components and mechanical characteristics [12][13].

The reference path as shown in Fig. 5 is given as follows: from A to B, the reference path is straight along with the x-axis; from B to C, the path is interpolated by the fifth-order polynomial of x; and from C to D, the path is defined as a straight path along with the x-axis again. The reference yaw orientation is defined as the angle between the x-axis and the tangent to the reference path.

The desired traveling velocity of the rover v_{d0} is given as 0.12 [m/s]. The slope angle of the surface is uniformly set as 10 [deg].

In the control strategy with the slip compensation, the control input for the path following u_p is distributed into both steering and driving maneuvers on front wheels, while the control input u_β is to the rear wheels to reduce the sideslip. Also, the reference slip ratio s_{ref} is given as 0.10 to compensate the longitudinal slip of wheels.

In case of the control not including the slip compensation, the control input u_p is employed into both steering and driving maneuvers of all wheels. Also, the slip ratios s_i and slip angles β_i are assumed to be zero.

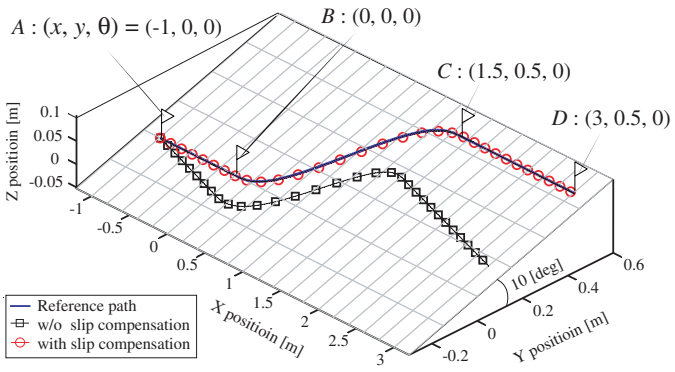

Fig. 5. Simulation result in slope case : path following

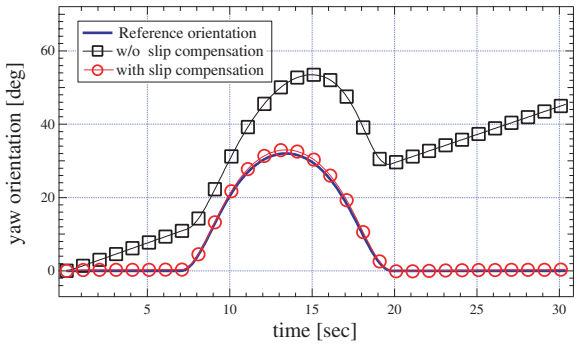

Fig. 6. Simulation result in slope case : yaw orientation

TABLE I
FINAL STATE ERRORS

	distance error [m]	orientation error [deg]
w/o slip compensation	0.383	46.2
w/ slip compensation	0.004	0.32

C. Simulation result and discussion

The simulation result regarding the path following is shown in Fig. 5. Also, Fig. 6 describes the time history of the yaw orientation of the rover. The final state error in both control are summarized in Table I. According to the result, it is clearly seen that the control with slip compensation is able to follow the desired path within a negligible error. On the other hand, control without slip compensation diverges from the desired path, as the slip motion of the rover is significant. As shown in Fig. 7, the proposed control can successfully diminish the slip ratio. Thus, it is shown that slip compensated control is necessary to follow the reference path on loose soil, particularly in the slope traveling situation.

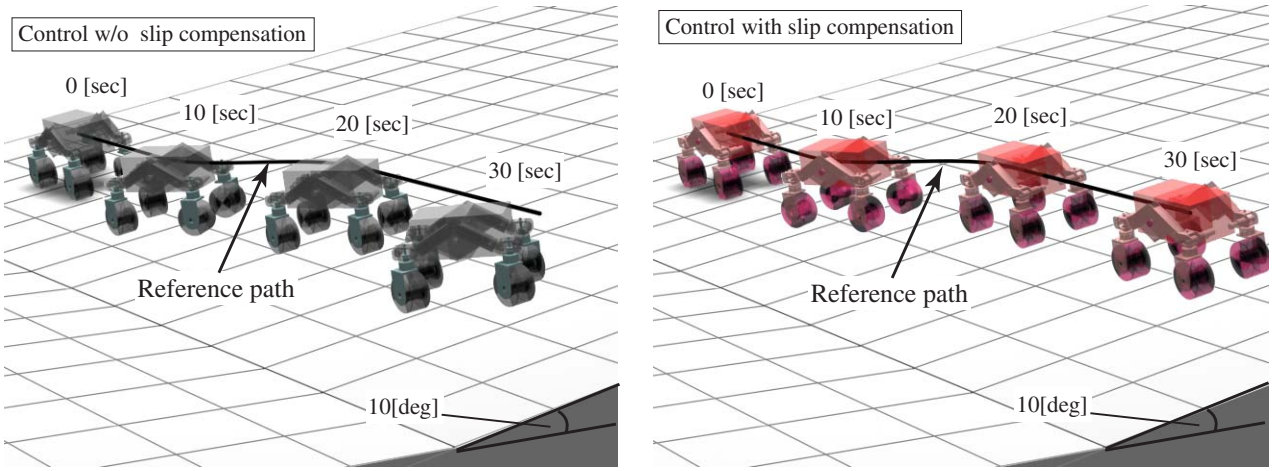

Fig. 8. Comparison of the rover's behavior on slope (left figure : control w/o slip compensation / right figure : control with slip compensation)

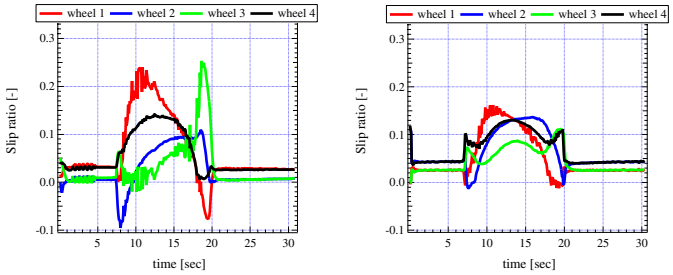

(w/o slip compensation) (w/ slip compensation)

Fig. 7. Simulation result : time profile of slip ratio

Fig. 8 presents the results of the simulation using computer graphics. It can be seen that steering maneuvers in the slip compensated control allow the rover to successfully follow the reference path.

VI. Conclusion and Future Works

In this paper, the path following control with slip compensation has been addressed. The proposed strategy was able to derive both steering and driving maneuvers of the rover, allowing it to follow an arbitrary path while to simultaneously compensate for slip. Through the simulation study, it was found that the proposed control shows much better performance than the control without slip compensation. Experiments should be conducted with applying the following approaches in order to discuss the feasibility (such as computational time or sensitivity of the sensor measurements) of the proposed strategy.

To apply the control strategy to a rover in practical situation, there are two main approaches: In the first approach, the rover is controlled to follow a path based on the proposed algorithm in real-time. A key issue in this approach is how to measure the traveling velocity of the rover, as the proposed control needs to monitor slip behavior. Typical techniques to measure the velocity are, for example, to use an accelerometer or an IMU (Inertial Measurement Unit) as internal sensors, and also an RTK-GPS (Real Time Kinematic-GPS), or an LMS (Laser Measurement System) as external sensors. In the second approach, the rover is maneuvered based on a motion profile which has been generated from the dynamics simulation in advance, since, the simulation model described on this paper has been proven to be sufficiently reliable to deal with the behavior of a real rover on loose soil.

References

[1] http://marsrovers.jpl.nasa.gov/home/index.html (as of February 2006)
[2] I. Nakatani, K. Matsumoto and T. Izumi; "SELENE-B: Proposed Lunar Mission with Lander and Rover," Proc. of the 7th Int. Symp. on Artificial Intelligence, Robotics and Automation in Space, 2003.
[3] R. Volpe and S. Peters; "Rover Technology Development and Infusion for the 2009 Mars Science Laboratory Mission," Proc. of the 7th Int. Symp. on Artificial Intelligence, Robotics and Automation in Space, 2003.
[4] K. Rajan, et al.; "MAPGEN: Mixed Initiative Planning and Scheduling for the Mars '03 MER Mission," Proc. of the 7th Int. Symp. on Artificial Intelligence, Robotics and Automation in Space, 2003.
[5] A. De Luca, G. Oriolo and C. Samson; "Feedback Control of a Nonholonomic Car-like Robot, *Robot Motion Planning and Control*',' edtied by J.-P Laumond, Springer-Verlag, 1998.
[6] C. C. de Wit, H. Khennouf, C. Samson and O. J. Sordalen; "Nonlinear Control Design for Mobile Robots, *Recent Trends in Mobile Robots*," edited by Y. F. Zheng, World Scientific Series in Robotics and Automated Systems, vol.11, 1993.
[7] S. Rezaei, J. Guivant and E. M. Nebot; "Car-Like Robot Path Following in Large Unstructured Environments," Proc of the 2003 IEEE Int. Conf. on Intelligent Robots and Systems, pp. 2468-2473, 2003.
[8] D. M. Helmick et al.; "Path Following using Visual Odometery for a Mars Rover in High-Slip Environments," Proc. of the 2004 IEEE Aerospace Conference, pp. 772 - 789, 2004.
[9] M. G. Bekker; "Introduction to Terrain-Vehicle Systems," The University of Michigan Press, 1969.
[10] J. Y. Wong; "Theory of Ground Vehicles," John Wiley & Sons, 1978.
[11] K. Iagnemma and S. Dubowsky; "Mobile Robot in Rough Terrain," Springer Tracts in Advanced Robotics, vol.12, 2004.
[12] K. Yoshida and G. Ishigami; "Steering Characteristics of a Rigid wheel for Explaration on Loose Soil," Proc of the 2004 IEEE Int. Conf. on Intelligent Robots and Systems, pp. 3995–4000, 2004.
[13] G. Ishigami and K. Yoshida; "Steering Characteristics of an Exploration Rover on Loose Soil Based on All-Wheel Dynamics Model," Proc of the 2005 IEEE Int. Conf. on Intelligent Robots and Systems, pp. 2041-2046, 2005.
[14] G. Ishigami, A. Miwa and K. Yoshida; "Steering Trajectory Analysis of Planetary Exploration Rovers Based on All-Wheel Dynamics Model," Proc. of the 8th Int. Symp. on Artificial Intelligence, Robotics and Automation in Space, 2005.